

Identification of modulating residues defining the catalytic cleft of insulin-regulated aminopeptidase

Siying Ye, Siew Yeen Chai, Rebecca A. Lew, David B. Ascher, Craig J. Morton, Michael W. Parker, and Anthony L. Albiston

Abstract: Inhibition of insulin-regulated aminopeptidase (IRAP) has been demonstrated to facilitate memory in rodents, making IRAP a potential target for the development of cognitive enhancing therapies. In this study, we generated a 3-D model of the catalytic domain of IRAP based on the crystal structure of leukotriene A4 hydrolase (LTA4H). This model identified two key residues at the 'entrance' of the catalytic cleft of IRAP, Ala427 and Leu483, which present a more open arrangement of the S1 subsite compared with LTA4H. These residues may define the size and 3-D structure of the catalytic pocket, thereby conferring substrate and inhibitor specificity. Alteration of the S1 subsite by the mutation A427Y in IRAP markedly increased the rate of substrate cleavage V of the enzyme for a synthetic substrate, although a corresponding increase in the rate of cleavage of peptide substrates Leu-enkephalin and vasopressin was not apparent. In contrast, [L483F]IRAP demonstrated a 30-fold decrease in activity due to changes in both substrate affinity and rate of substrate cleavage. [L483F]IRAP, although capable of efficiently cleaving the N-terminal cysteine from vasopressin, was unable to cleave the tyrosine residue from either Leu-enkephalin or Cyt6-desCys¹-vasopressin (2–9), both substrates of IRAP. An 11-fold reduction in the affinity of the peptide inhibitor norleucine¹-angiotensin IV was observed, whereas the affinity of angiotensin IV remained unaltered. In addition we predict that the peptide inhibitors bind to the catalytic site, with the NH₂-terminal P1 residue occupying the catalytic cleft (S1 subsite) in a manner similar to that proposed for peptide substrates.

Key words: angiotensin IV, IRAP, aminopeptidase, enzyme inhibitors.

Résumé : L'inhibition de l'aminopeptidase régulée par l'insuline (IRAP) facilite la mémoire et ce faisant, fait de l'IRAP une cible potentielle du développement de thérapies visant à améliorer les fonctions cognitives. Dans cette étude, nous avons généré un modèle en trois dimensions du domaine catalytique de l'IRAP sur la base de la structure de la leukotriène A4 hydrolase (LTA4H). Ce modèle a permis d'identifier deux résidus, l'Ala427 et la Leu483 à l'entrée du sillon catalytique de l'IRAP qui présentent un arrangement plus ouvert dans le sous-site S1 comparativement à ce qui est observé avec la LTA4H. Ces résidus peuvent définir la taille et la structure tridimensionnelle de la poche catalytique qui confère la spécificité au substrat et aux inhibiteurs. L'altération du sous-site S1 par la mutation A427Y chez l'IRAP augmente fortement le taux de clivage du substrat de l'enzyme V pour un substrat synthétique, quoiqu'une augmentation correspondante du taux de clivage de substrats peptidiques, la Leu-enképhaline et la vasopressine ne soit pas apparent. En revanche, une augmentation de 30 fois de l'activité de l'IRAP L483F a été observée, à cause de changements de l'affinité et le taux de clivage du substrat. L'IRAP L483F, même si elle était capable de cliver efficacement la cystéine N-terminale de la vasopressine était incapable de cliver le résidu tyrosine de la Leu-enképhaline ou de la vasopressine Cyt6-desCys¹, tous deux substrats de l'IRAP. Une diminution de 11 fois de l'affinité du peptide inhibiteur norleucine¹-angiotensine IV a été observée alors que l'affinité de l'angiotensine IV n'était pas affectée. De plus, nous prédisons que les peptides inhibiteurs se lient au site catalytique, le résidu NH₂-terminal P1 occupant le sillon catalytique (sous-site S1) de façon similaire à celle proposée pour les peptides substrats.

Received 20 December 2007. Accepted 14 March 2008. Published on the NRC Research Press Web site at bc.b.nrc.ca on 27 May 2008.

Abbreviations: A-LAP, adipocyte-derived leucine aminopeptidase; APA, aminopeptidase A; APN, aminopeptidase N; Ang IV, angiotensin IV; AT4, angiotensin IV receptor; GLUT4, glucose transporter 4; HEK, human embryonic kidney; IRAP, insulin-regulated aminopeptidase; L-RAP, leukocyte-derived arginine aminopeptidase; LTA4H, leukotriene A4 hydrolase; LVV-H7, LVV-hemorphin 7; P-LAP, placental leucine aminopeptidase; TRH-DE, thyrotropin-degrading enzyme.

S. Ye and A.L. Albiston.¹ Howard Florey Institute, Florey Neurosciences Institutes, University of Melbourne, Parkville, Victoria 3010, Australia.

S.Y. Chai. Howard Florey Institute, Florey Neurosciences Institutes, University of Melbourne, Parkville, Victoria 3010, Australia; Centre for Neuroscience, University of Melbourne, Parkville, Victoria 3010, Australia.

R.A. Lew. Department of Biochemistry and Molecular Biology, Monash University, Clayton, Victoria 3800, Australia.

D.B. Ascher and C.J. Morton. St Vincent's Institute of Medical Research, Fitzroy, Victoria 3065, Australia.

M.W. Parker. St Vincent's Institute of Medical Research, Fitzroy, Victoria 3065, Australia; Department of Biochemistry and Molecular Biology, University of Melbourne, Parkville, Victoria 3010, Australia.

¹Corresponding author (e-mail: anthony.albiston@florey.edu.au).

Mots-clés : angiotensine IV, IRAP, aminopeptidase, inhibiteurs d'enzyme.

[Traduit par la Rédaction]

Introduction

Alzheimer's disease is the most common cause of dementia; however, other causes of cognitive impairment include perinatal brain injury, cerebrovascular disease, cardiac surgery, hypotension, anoxia, traumatic brain injury, and other neurodegenerative diseases. It is estimated that 15% of people over the age of 65 suffer from some form of memory impairment. Currently, there is no effective treatment for memory loss. We have identified a potential new target, insulin-regulated aminopeptidase (IRAP; EC 3.4.11.3), which would be useful in the development of therapeutic drugs for treating memory loss (Albiston et al. 2001).

Infusion of the peptide inhibitors of IRAP, angiotensin IV (Ang IV), and LVV-hemorphin-7 (LVV-H7) into the brain facilitated memory retention and retrieval in rats in a range of spatial memory and aversive conditioning paradigms (Braszko et al. 1988; Wright et al. 1993; Wright et al. 1999; Chai et al. 2001; Lee et al. 2004). Furthermore, in different rat models of amnesia, IRAP inhibitors ameliorate the performance deficits. Memory impairments due to scopolamine and mescaline treatment (Pederson et al. 1998; Olson et al. 2004), ischemic damage (Krebs et al. 1996), chronic alcohol exposure (Wisniewski et al. 1993), and bilateral perforant pathway lesions (Krishnan et al. 1999) have all been successfully attenuated by treatment with IRAP inhibitors.

Currently Ang IV, LVV-H7, and their derivatives are the only high-affinity inhibitors of IRAP available. They bind selectively to IRAP and display competitive kinetics in inhibiting the enzyme activity of the recombinant enzyme *in vitro* (Lew et al. 2003). This strongly suggests that the peptides mediate their memory effects by binding to the catalytic site of IRAP and blocking its activity. IRAP can cleave a range of peptide hormones efficiently *in vitro*, including oxytocin (OXY), vasopressin (AVP), enkephalin (Enk), somatostatin, and dynorphin (Lew et al. 2003; Herbst et al. 1997). A recent study using IRAP knockout mice suggests that AVP may be metabolized by IRAP *in vivo* (Wallis et al. 2007). To provide important insights into the mechanism of action of these peptide inhibitors, we investigated the catalytic site of IRAP in relation to the binding of the peptide inhibitors and putative substrates.

IRAP belongs to the M1 family of zinc metallopeptidases consisting of 13 mammalian members, including leukotriene A4 hydrolase (LTA4H; EC 3.3.2.6), aminopeptidase A (APA; EC 3.4.11.7), and aminopeptidase N (APN; EC 3.4.11.2). This class of enzymes shows high similarity in the primary structure of the catalytic domain, which contains two consensus motifs: a zinc-binding HEXXH(X)₁₈E motif and an exopeptidase GXMEN motif. Based on the crystal structure of LTA4H (Thunnissen et al. 2001), we generated a homology model of the catalytic domain of human IRAP from residues Leu150–Ser533 to investigate the interactions of IRAP with its inhibitors and substrates. Analysis of the model of IRAP reveals an important difference conferred by

residues Ala427 and Leu483 at the catalytic cleft, corresponding to residues Tyr267 and Phe314 in LTA4H. According to our model, the Ala427 and Leu483 residues create a wider opening to the catalytic cleft of IRAP, resulting in a more open arrangement of the S1 subsite, in contrast to the bulky side-chains in the corresponding LTA4H residues. This difference may be involved in determining the substrate specificity of IRAP and potentially, in the capacity of the enzyme to cleave different N-terminal amino acids. In this paper we demonstrate that mutation of residues Ala427 and Leu483 in IRAP, replacing them with the corresponding residues in LTA4H, significantly alters the aminopeptidase activity of the enzyme. In addition, for the different mutants, we observed selective changes in their ability to cleave peptide substrates and bind peptide inhibitors. These differences correlated with the differences in the amino termini of the substrates and inhibitors, thus identifying a key role for Ala427 and Leu483 residues in defining the S1 subsite of the catalytic site of IRAP.

Materials and methods

Materials

Ang IV, Nle¹-Ang IV, LVV-H7, (Arg⁸)-AVP and Leu-enkephalin (Leu-Enk) were purchased from Auspep (Melbourne, Australia). The fluorescent substrate L-leucine-4-methyl-7-coumarinylamide (Leu-MCA), its cleavage product 7-amino-4-methylcoumarin (MCA), and all other reagents were purchased from Sigma (Castle Hill, NSW, Australia).

Molecular modeling of the catalytic site of IRAP

The protease domain of IRAP (residues Leu140–Ser533) was modelled on the structure of the equivalent domain of LTA4H (residues Ser8–Leu389, PBD code 1HS6) (Thunnissen et al. 2001). Although the overall identity between the sequences is low, the region immediately surrounding the active site residues, including the HEXXH and GXMEN motifs, is relatively well conserved, with 41% sequence identity. A sequence alignment of the catalytic domains of several different members of the M1 aminopeptidase family, including IRAP and LTA4H, was used to guide model building (data not shown). The model was built using COMPOSER in Sybyl6.8 (Tripos Inc., St Louis, Missouri, USA) and minimized in Sybyl6.8 under the Tripos forcefield with the final structure having more than 95% of residues in the allowed region of a Ramachandran plot. Zinc was manually added to the active site motif after comparison with the zinc-bound LTA4H structure indicated the conformation of residues in the zinc binding motif was effectively identical in the two proteins. The quality of the model was confirmed with Verify3D (Eisenberg et al. 1997), which indicated that the model was of good quality (data not shown). Model structures were examined using Sybyl6.8. Models of the IRAP mutants were built using the same approach.

Leu-MCA docking into the models of the mutants was performed using AutoDock 3.0 (Morris et al. 1998), with a grid size of $60 \times 60 \times 80$ and a grid spacing of 0.375 \AA . The zinc parameters for AutoDock 3 were the optimized parameters (zinc radius, 0.87 \AA ; well depth, 0.35 kcal/mol ; and zinc charge, $+0.95e$) taken from Hu and Shelver (2003). Step sizes were 1 \AA for translation and 50° for rotation, and the number of energy evaluations was set to 2 000 000. One hundred Lamarckian genetic algorithm docking runs were performed and the results were analyzed in VMD (Humphrey et al. 1996).

Cell culture and transfection

HEK 293T cells were grown in Dulbecco's modified Eagle's medium (Trace Biosciences Pty. Ltd, New York, USA) supplemented with 10% heat-inactivated fetal calf serum (Trace Biosciences), 100 U/mL penicillin–streptomycin (Invitrogen www.invitrogen.com), 250 U/mL Fungizone (GIBCO), and 2 mmol/L glutamine (Trace Biosciences) at 37°C in 5% CO_2 . For transient expression, HEK 293T cells were transfected with either 20 μg pCIIRAP (wild-type IRAP, a gift from M. Tsujimoto, Riken, Wako, Japan) or the IRAP mutants, or empty vector using Lipofectamine transfection reagent (Invitrogen, California, USA), according to the manufacturer's instructions.

Site-directed mutagenesis

PCR-based site-directed mutagenesis was carried out with the QuickChange Site-Directed Mutagenesis Kit (Stratagene, La Jolla, California, USA), according to the manufacturer's instructions; we used the full-length cDNA encoding human IRAP construct in pCI-neo vector (pCI-IRAP) as the template. DNA sequencing with an Applied Biosystems 371 automated sequencer was used to verify mutations.

Protein determination

Protein concentration was determined with the DC Protein Assay kit (BioRad, California, USA) using bovine serum albumin as standard.

Western blot analysis

Membranes were prepared from cells as previously described (Lew et al. 2003). Samples were solubilized with 2% SDS under reducing conditions (with dithiothreitol), resolved by SDS – 7.5% polyacrylamide gel electrophoresis, and transferred onto SEQUI-BLOT PVDF membranes (BioRad). Western blot analysis was carried out with an anti-IRAP polyclonal antibody (raised against amino acids 25–47 of human IRAP) (Fernando et al. 2005), which was detected using horseradish-peroxidase-conjugated sheep anti-rabbit secondary antibody (Chemicon international, Temecula, California, USA) by means of an enhanced chemiluminescence method with ECL Western blotting detection reagents (Amersham Biosciences, Buckinghamshire, England). The immunoreactivity was captured using a luminescent image analyser, LAS-1000, Intelligent Dark Box II (FujiFilm, Kanagawa, Japan).

Enzymatic activity assay

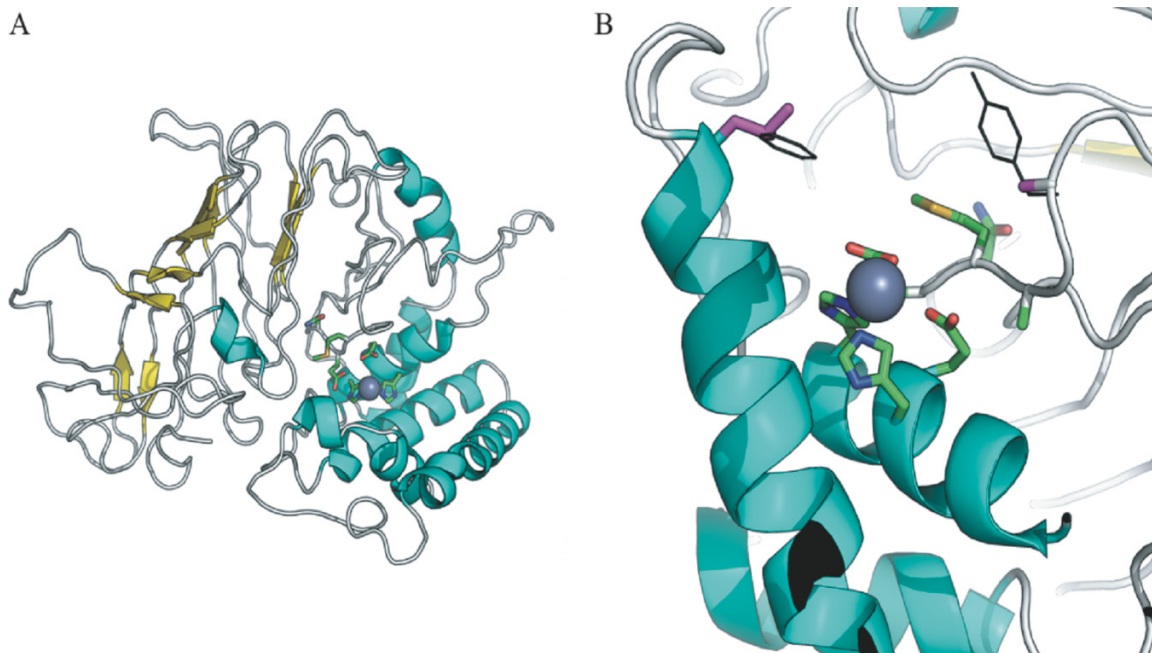
Samples for enzyme analysis were prepared as previously

described (Lew et al. 2003; Albiston et al. 2001). In brief, membranes were prepared from HEK 293T cells transfected with IRAP or the IRAP mutants, then solubilized in buffer consisting of 50 mmol/L Tris–HCl and 1% (v/v) Triton X-100 (pH 7.4) at 4°C with agitation over 5 h. After solubilization, the membranes were pelleted by centrifugation at 23 100g for 15 min at 4°C , and the supernatant was reserved as the source of IRAP activity. The enzymatic activities of wild-type IRAP and mutants were determined by hydrolyzing the synthetic substrate leucine-7-amido-4-methylcoumarin (Leu-MCA) (Sigma-Aldrich), which was monitored by the release of a fluorogenic product, MCA, at excitation and emission wavelengths of 380 and 440 nm, respectively. Assays were performed in 96-well plates; each well contained between 0.2 and 10 μg solubilized membrane protein, a range of concentration of substrate in a final volume of 100 μL of 50 mmol/L Tris–HCl buffer (pH 7.4). Nonspecific hydrolysis of the substrate was corrected by subtracting the emission from incubations with membranes transfected with empty vector. Reactions proceeded at 37°C for 30 min within a thermostatted FLEX station fluorescence microplate reader (Molecular Devices, Sunnyvale, California, USA). The kinetic parameters (K_m and V) were determined by nonlinear fitting of the Michaelis–Menten equation (GraphPad Prism, GraphPad Software Inc., San Diego, California, USA); final concentrations of Leu-MCA were $15.6 \mu\text{mol/L} - 1 \text{ mmol/L}$. Inhibitor constants (K_i) for the competitive inhibitors were calculated from the relationship $\text{IC}_{50} = K_i(1+[S]/K_m)$, where IC_{50} values were determined over a range of inhibitor concentrations ($10^{-9} - 10^{-4} \text{ mol/L}$). K_m values of wild-type and mutant IRAPs for Leu-MCA were determined from the kinetic studies. Binding affinities of IRAP substrates to wild-type or mutant IRAPs were examined by monitoring the inhibition of the hydrolysis of Leu-MCA in the presence of increasing concentrations of AVP ($10^{-8} - 10^{-3} \text{ mol/L}$) or Leu-Enk ($10^{-6} - 10^{-2} \text{ mol/L}$). All data obtained were from at least three separate experiments performed in duplicate.

Determination of substrate degradation

The degradation of substrates by wild-type or mutant IRAP was analysed using reverse-phase HPLC, as described previously (Lew et al. 2003). In brief, each peptide substrate (30 μg) was incubated at 37°C in Tris-buffered saline (100 mmol/L Tris–HCl, 150 mmol/L NaCl (pH 7.4)) with 10 μg solubilized membrane protein from HEK293T cells transfected with wild-type or mutant IRAP. At each time point (0, 0.5, 1, 2, 4, and 6 h), an aliquot containing 5 μg peptide was removed, and the reaction stopped by adding 4 volumes methanol – 1% trifluoroacetic acid (TFA). Samples were dried on a centrifugal vacuum evaporator (Speed-Vac, Savant, Farmingdale, New York, USA) prior to HPLC analysis using an Agilent 1100 series LC with an on-line mass spectrometric detector (Agilent Technologies, Palo Alto, California, USA). Samples were loaded onto a Zorbax Eclipse C18 column (maintained at 50°C) in 1.8% acetonitrile – 0.1% TFA n 0.02% acetic acid at 0.15 mL/min, and eluted with a 30 min linear gradient to 60% acetonitrile – 0.1% TFA. Fragments were identified

Fig. 1. Diagrammatic representation of the molecular model of the catalytic domain of human IRAP indicating the position of key features of the active site. (A) Overall structure of the IRAP model; the protein is shown as a schematic, with the position of the zinc atom indicated as a grey sphere. (In the online version, the schematic is coloured by secondary structure as follows: helices, cyan; strands, yellow; loops, white.) Residues contributing to the HEXXH and GXMEN motifs are shown as rods. (In the online version, the rods are coloured by atom type.) (B) A comparison of the active-site residues A427 and L483 in IRAP with Y267 and F314 in LTA4H. The homology model of the IRAP catalytic domain is shown as a schematic, with the HEXXH and GXMEN motifs shown as rods and the zinc atom shown as a grey sphere. (In the online version, the schematic is coloured by secondary structure, with the HEXXH and GXMEN motifs coloured by atom type.) A427 and L483 from IRAP are shown as black rods (residues at top of panel) with the residues at the equivalent positions in LTA4H, Y267 and F314 respectively, shown as dark grey lines. (In the online version, A427 and L483 from IRAP are shown as magenta rods.) The substitution of the two bulky aromatic side chains in LTA4H, which occlude the top of the active site, with the much smaller alkyl side-chains in IRAP substantially alters the shape of the active site with a concomitant effect of substrate specificity. This figure was produced with PyMOL.



following mass spectral analysis using Agilent ChemStation deconvolution software.

Results

Molecular modelling of the catalytic domain of IRAP

The molecular model of the catalytic domain of IRAP (Leu150–Ser533) was built using the catalytic domain of LTA4H as a template (Fig. 1). The relatively high conservation of residues around the active site zinc suggests that this region of the model will be the most reliable (Fig. 2). Subsequently, differences between IRAP and LTA4H in the residues in the catalytic site have the potential to provide insight into the functional differences between the two proteins.

Analysis of the model of the catalytic cleft of IRAP and LTA4H reveals an important difference conferred by two amino acids, residues Ala427 and Leu483 in IRAP, compared with that conferred by the corresponding residues Tyr267 and Phe314 in LTA4H. The aromatic side chains in Tyr267 and Phe314 narrow the opening of the catalytic cleft of LTA4H, distinguishing it from the relatively open arrangement in IRAP created by Ala427 and Leu483 (Fig. 1).

Mutagenesis and expression of recombinant IRAPs

To investigate the functional and structural roles of

Ala427 and Leu483, we used site-directed mutagenesis to replace them with the corresponding LTA4H residues Tyr267 and Phe314, respectively, to generate the single mutations [A427Y]IRAP and [L483F]IRAP, and the double mutation [A427Y/L483F]IRAP. Western blot analysis of membrane proteins from HEK 293T cells transiently transfected with wild-type or mutant IRAPs demonstrated that all four constructs were expressed at a similar level and with the same molecular mass, indicating that none of the mutations affected the biosynthesis or processing of IRAP (Fig. 3). The two bands observed for IRAP were due to differential glycosylation, as digestion of IRAP membranes with PNGase F resulted in a reduction in the size of both IRAP monomers to 140 kDa (results not shown).

Determination of enzyme kinetics using the synthetic substrate Leu-MCA

[A427Y]IRAP

The enzymatic activity of IRAP against the synthetic substrate Leu-MCA was significantly enhanced by the substitution of Ala427 with tyrosine compared with the activity of wild-type IRAP (Table 1). In our assay system, substrate depletion was a problem for this mutant and we therefore performed the analysis with a 10-fold lower enzyme concentration to achieve a linear time – product relationship

Fig. 2. Sequence alignment of the catalytic domain of the human M1 aminopeptidases. Shown is an alignment of the amino acid sequences of adipocyte-derived leucine aminopeptidase (A-LAP; EC 3.4.11.-), leukocyte-derived arginine aminopeptidase (L-RAP; EC 3.4.11.-), IRAP (EC 3.4.11.3), aminopeptidase A (APA; EC 3.4.11.7), puromycin-sensitive aminopeptidase (PSA; EC 3.4.11.14), aminopeptidase N (APN; EC 3.4.11.2), thyrotropin-releasing hormone-degrading ectoenzyme (TRH-DE; EC 3.4.19.6), aminopeptidase B (APB; EC 3.4.11.6), and leukotriene A4 hydrolase (LTA4H; EC 3.3.2.6). The conserved GAMEN and HEXXXH18E motifs are boxed, and A427 and L483 in the IRAP sequence are indicated with arrows. The sequence alignment was created using T-coffee (Notredame et al. 2000).



during the assay. Kinetic studies were then performed to determine the kinetic parameters (K_m and V) of [A427Y]IRAP. At high concentrations of the synthetic substrate, Leu-MCA (>125 $\mu\text{mol/L}$), the rates of substrate hydrolysis were considerably decreased (Fig. 4). This effect may be due to substrate inhibition, with the rate of substrate hydrolysis v described by

$$[1] \quad v = V \div (1 + (K_m \div ([S] \times K_{si})))$$

where V , K_m , and $[S]$ represent the maximal velocity, Michaelis–Menten constant, and total substrate concentration, respectively, and K_{si} is the equilibrium constant for substrate inhibition. The experimental data for [A427Y]IRAP (Fig. 4) fit this equation, and suggest substrate inhibition at higher concentrations. Therefore, the kinetic parameters for the cleavage of Leu-MCA by [A427Y]IRAP were determined using eq. 1 with the full range of substrate concentrations (15.625 $\mu\text{mol/L}$ – 1 mmol/L) (Table 1). The replacement of Ala427 with tyrosine had a minor effect on the K_m value but significantly increased the V values by 3-fold, resulting in a 4.3-fold increase in the V/K_m ratio compared with that of wild-type IRAP.

[L483F]IRAP and [A427Y/L483F]IRAP

In contrast to [A427Y]IRAP, there was no detectable activity for the L482F mutant when 2 μg membrane proteins per well was used. To determine the kinetic parameters of this mutant, levels of protein that were 4-fold higher than those of wild-type IRAP were used in the assay. In a similar manner to [A427Y]IRAP, the rates of substrate hydrolysis considerably decreased at higher concentrations of the sub-

strate, indicative of substrate inhibition (Fig. 4). Therefore, we used eq. 1 to calculate the kinetic parameters. The V/K_m ratio obtained for [L483F]IRAP was 30-fold lower than that obtained for wild-type IRAP (Table 1). No enzyme activity was detected for the double mutant [A427Y/L483F]IRAP at a range of concentrations tested (2–10 μg) in the assay system (data not shown).

Degradation of peptide substrates AVP and Leu-Enk

A427Y]IRAP

The A427Y mutation resulted in a decrease of approximately 70% in activity towards the peptide substrate AVP. In contrast, Leu-Enk was degraded by [A427Y]IRAP at the same rate as that by wild-type IRAP (Table 2). The binding affinities of the peptide substrates for wild-type and mutant IRAPs were also determined by inhibition assays measuring the degradation of the synthetic substrate (25 $\mu\text{mol/L}$ Leu-MCA) in the presence of increasing concentrations of AVP or Leu-Enk. Both AVP and Leu-Enk demonstrated marked increases in affinity (5- and 26-fold, respectively) for [A427Y]IRAP compared with that for wild-type IRAP (Table 3 and Fig. 5). Although the affinity of the peptide substrates for [A427Y]IRAP increased, the degradation rate of AVP decreased and remained unaltered for Leu-Enk compared with wild-type IRAP.

[L483F]IRAP and [A427Y/L483F]IRAP

The [L483F] mutant IRAP cleaved AVP with the same efficiency as wild-type IRAP (Table 2). However, wild-type IRAP generates two products, Cyt6-AVP(2–9) and Cyt6-AVP(3–9), by sequentially cleaving the first and second peptide bonds of AVP, whereas [L483F]IRAP only cleaved

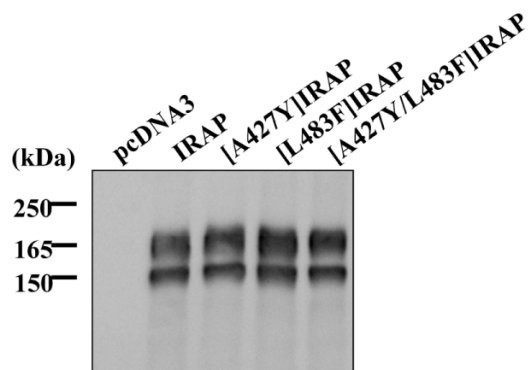
Table 1. Kinetic parameters for the hydrolysis of Leu-MCA by wild-type IRAP and mutants of predicted key residues.

| Enzyme | K_m , $\mu\text{mol/L}$ | V , ($\mu\text{mol}/(\text{L} \cdot \mu\text{g} \cdot \text{h})$) | V/K_m , ($\mu\text{g} \cdot \text{h})^{-1}$ |
|--------------------------|---------------------------|---|--|
| IRAP | 38.7 ± 3.1 | 114.3 ± 10.5 | 3.0 ± 0.3 |
| [A427Y]IRAP ^a | 27.3 ± 3.5 | $356.5 \pm 29.5^*$ | $13.0 \pm 1.1^*$ |
| [A427Y]IRAP ^b | 28.2 ± 3.1 | $352.8 \pm 31.9^*$ | $12.0 \pm 1.1^*$ |
| [L483F]IRAP ^a | $68.0 \pm 5.7^*$ | $6.4 \pm 1.5^*$ | $0.1 \pm 0.02^*$ |
| [L483F]IRAP ^b | $199.7 \pm 45.8^*$ | $16.7 \pm 4.1^*$ | $0.08 \pm 0.02^*$ |
| [A437Y/L483F]IRAP | No activity | No activity | No activity |

Note: K_m and V values are the means \pm SE of at least four individual experiments with duplicate determinations. *, Statistically significant at $p < 0.01$ (mutant IRAPs vs wild type).

^aKinetic parameters that were obtained from the best fit of the Michaelis–Menten equation (the concentrations of Leu-MCA were 15.625–125 $\mu\text{mol/L}$ for [A427Y]IRAP and 15.625–250 $\mu\text{mol/L}$ for [L483F]IRAP, respectively).

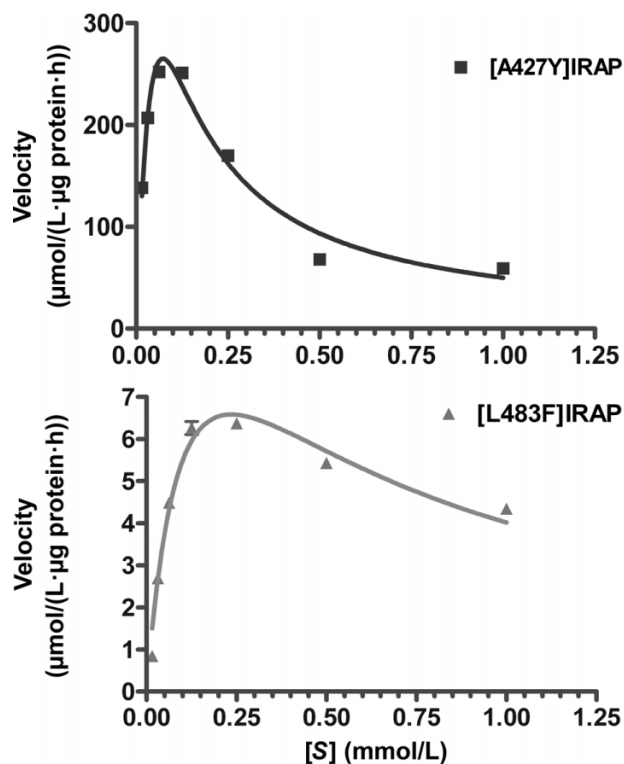
^bKinetic parameters that were obtained from the best fit of eq. 1 (the concentrations of Leu-MCA were 15.625 $\mu\text{mol/L}$ – 1 mmol/L).

Fig. 3. Western blot analysis of empty vector pcDNA3, wild-type IRAP, [A427Y]IRAP, [L483F]IRAP, and [A437Y/L483F]IRAP transiently expressed in HEK 293T cells. Membrane proteins (10 μg) were solubilized in 2% SDS under reducing conditions and resolved by SDS – 7.5% polyacrylamide gel electrophoresis.

the first peptide bond and therefore no Cyt6-AVP(3–9) was generated. In addition, no degradation of Leu-Enk by [L483F]IRAP was observed (Table 2). Therefore, [L483F]IRAP was unable to cleave Leu-Enk or Cyt6-AVP(2–9), both substrates of IRAP that have a tyrosine at the N terminus. The affinity of Leu-Enk for [L483F]IRAP obtained from the inhibition assay was identical to that of wild-type IRAP; therefore, the lack of degradation is not due to an alteration in affinity for the substrate. In contrast, the affinity of AVP for [L483F]IRAP was 6-fold higher than that for IRAP, which may compensate for a lower velocity as observed for [L483F]IRAP using the synthetic substrate, resulting in the unaltered degradation capacity observed for this mutant. As with the synthetic substrate, no cleavage of the peptide substrates was observed for the double mutant [A427Y/L483F]IRAP (Table 2).

Inhibition by peptide inhibitors and bestatin

Enzyme inhibition assays were carried out to investigate the effect of the mutations on the binding affinity of IRAP inhibitors. For [A427Y]IRAP, we did not observe any significant difference in K_i values for any of the peptide inhibitors (Table 4). However, the affinity of bestatin increased 8.2-fold compared with that of wild-type IRAP. In contrast,

Fig. 4. Substrate inhibition of [A427Y]IRAP and [L483F]IRAP. Hydrolysis of synthetic substrate Leu-MCA was measured as fluorescence units, as described in Materials and methods. Initial velocity rates are plotted as a function of substrate concentration, [S]. Solid lines represent the best fits of eq. 1 to the experimental data.

the L483F mutation resulted in significant decreases in the affinities of Nle¹-Ang IV and LVV-H7 by 11- and 2.1-fold, respectively, and an over 4-fold decrease in the affinity of bestatin. However, the inhibitory effect of Ang IV was unaltered (Table 4).

Docking of synthetic and peptide substrates into models of wild-type and mutant IRAP

The crystal structures of several M1 aminopeptidases have been solved, including those for leukotriene A4 hydrolase and aminopeptidase N (Thunnissen et al. 2001 and Ito et al. 2006, respectively). The interactions observed between the

Table 2. Degradation of AVP and Leu-enkephalin by wild-type IRAP, [A427Y]IRAP, [L483F]IRAP, and [A427Y/L483F]IRAP.

| Enzyme | Vasopressin (AVP) $\overline{\text{CYFQNCPRG}}$ | Leu-Enk YGGFL |
|--------------------|---|------------------|
| IRAP | 1.0 | 1.0 |
| [A427Y]IRAP | 0.3 | 1.0 |
| [L483F]IRAP | 1.0 ^a | No activity |
| [A427Y/ L483F]IRAP | No activity | No activity |

^aOnly Cyt6-AVP(2–9) was generated.

Table 3. Inhibition of the catalytic activities of wild-type IRAP, [A427Y]IRAP, and [L483F]IRAP by the substrates AVP and Leu-enkephalin.

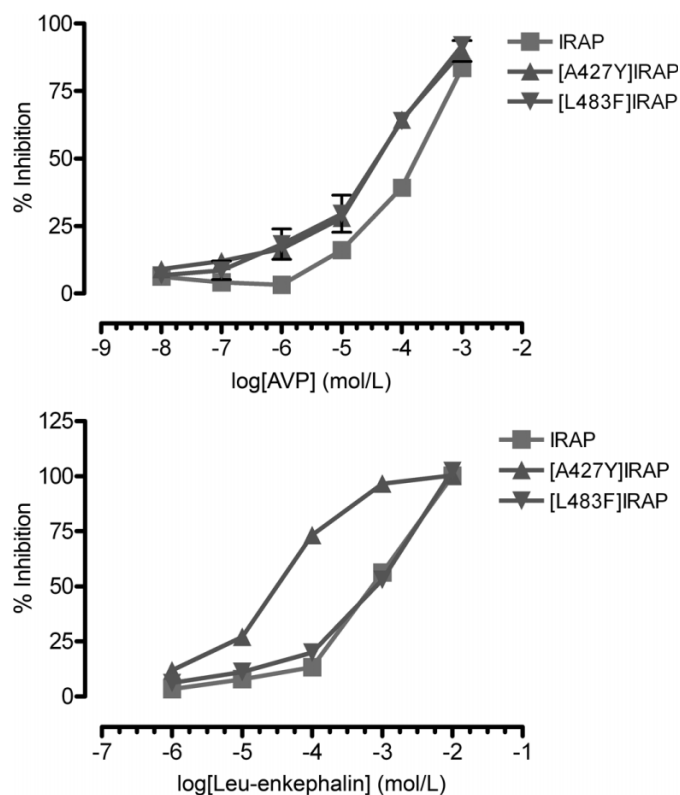
| Enzyme | K_i ($\mu\text{mol/L}$) | |
|--------------------|-----------------------------|------------------|
| | AVP | Leu-enkephalin |
| IRAP | 157.7 \pm 56 | 676 \pm 58 |
| [A427Y]IRAP | 29.5 \pm 3.6* | 26.4 \pm 1.3** |
| [L483F]IRAP | 40.6 \pm 10* | 972 \pm 277 |
| [A427Y/ L483F]IRAP | No activity | No activity |

Note: Values represent means \pm SE. K_i was calculated from the relationship $\text{IC}_{50} = K_i(1+[S]/K_m)$ with the K_m values obtained from Table 1 and $[S] = 25 \mu\text{mol/L}$. *, Statistically significant at $p < 0.05$; **, statistically significant at $p < 0.01$ (mutant IRAPs vs the wild type).

fluorogenic substrate Leu-MCA and the active site residues of our model of wild-type IRAP after computational docking (Figs. 6A and 6B) were consistent with the biochemical mechanism described by Ito et al. (2006) in their description of the M1 aminopeptidase aminopeptidase N, wherein proton donation by Tyr529 of IRAP completes hydrolysis of the N-terminal peptide bond.

Docking studies of Leu-MCA into models of the A427Y and L483F mutants suggest that these interactions are perturbed in the mutant proteins. For the L483F mutant, there are two main families of docking solutions with nearly equivalent binding affinities. The first solution is essentially identical to the wild-type conformation, with Tyr529 within hydrogen bonding distance of the carbonyl oxygen. In the alternate solution, the substrate is rotated by approximately 90° such that the carbonyl oxygen is no longer in close proximity to Tyr529. The alternate conformation is unlikely to be productive because the hydrogen bond to the tyrosine side chain (which is now lost) plays a critical role in stabilizing the reaction intermediate (Fig. 6C). We propose that the presence of an alternate binding conformation of similar affinity to the enzymatically productive orientation reduces the rate of MCA hydrolysis by the L483F mutant enzyme.

Modelling of the A427Y mutant was complicated by the fact that the active site could accommodate either of the two alternate common rotamers of the aromatic side chain. One of the rotamers protrudes into the space immediately surrounding the active site zinc, thereby preventing substrate from docking in its normal position close to the zinc ion. This model conflicts with our experimental evidence, which showed a greater turn-over rate of Leu-MCA by the A427Y enzyme compared with that of the wild type. A model incorporating the other tyrosine rotamer, which fits within the ac-

Fig. 5. Inhibition of the catalytic activities of wild-type IRAP, [A427Y]IRAP, and [L483F]IRAP by the substrates AVP and Leu-enkephalin. Aminopeptidase activities of wild-type IRAP, [A427Y]IRAP, and [L483F]IRAP were determined at a concentration of 25 $\mu\text{mol/L}$ Leu-MCA in the absence or presence of AVP (10^{-8} – 10^{-3} mol/L) or Leu-nkephalin (10^{-6} – 10^{-2} mol/L). Values are expressed as the percent inhibition of substrate cleavage relative to control, and are the means \pm SE of at least three independent experiments, each performed in duplicate.

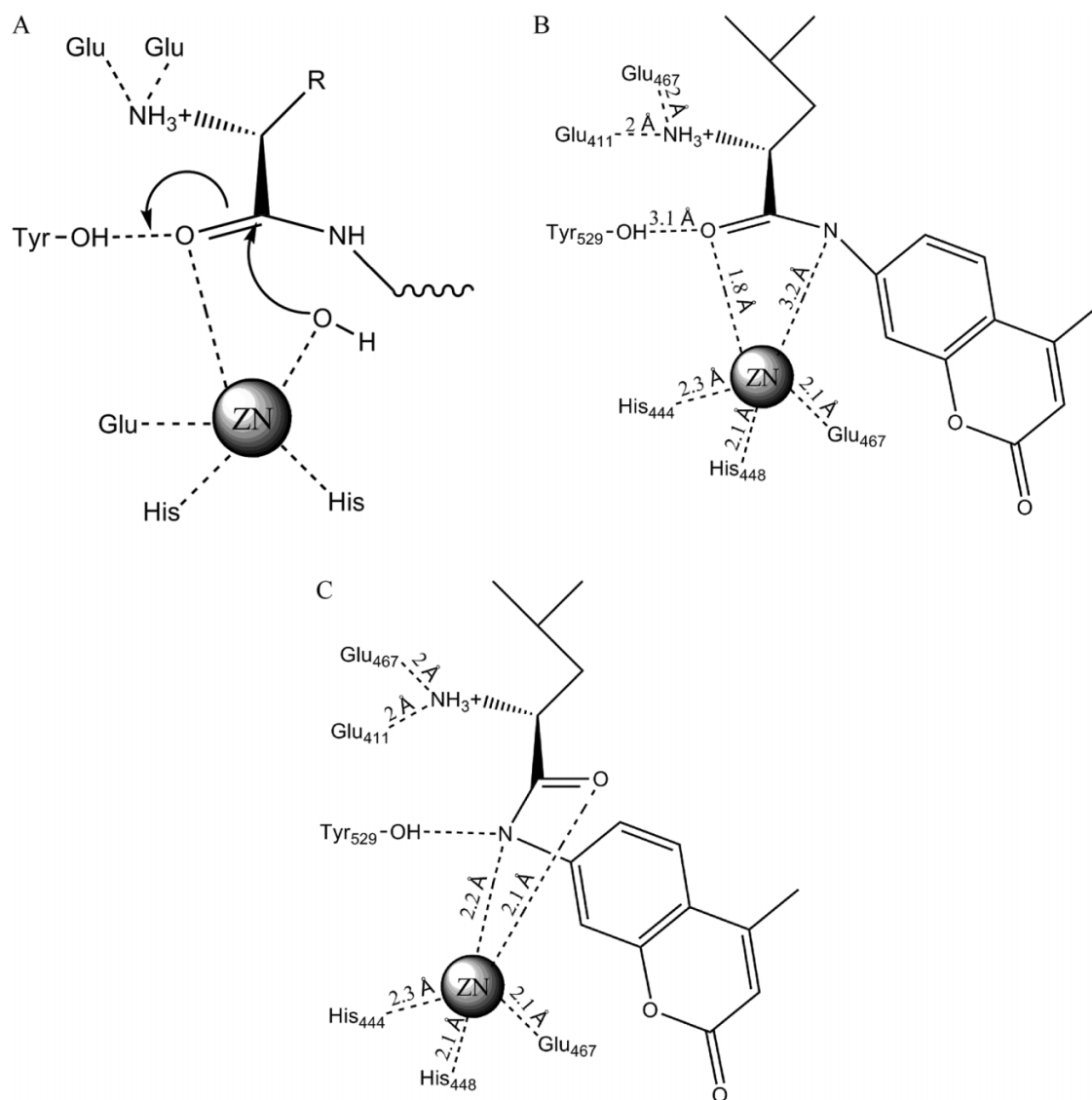
tive site of IRAP, leaves the active site zinc accessible to Leu-MCA during docking. As predicted, the tyrosine side chain still restricts the size of the active site when it adopts this rotamer in a manner likely to block the processing of cyclic peptides and other more bulky substrates. This is supported by the experimental data showing a loss of activity for the A427Y enzyme against peptide substrates. Consistent with the observation that Leu-MCA was able to dock into the models for both of the single mutants, the compound was also able to dock into our model of the double mutant, provided that Tyr427 was in the enzymatically productive rotamer. This conflicts with our experimental evidence,

Table 4. K_i values of AT4 peptide inhibitors and bestatin for wild-type IRAP and the [A427Y]IRAP, [L483F]IRAP, and [A427Y/L483F]IRAP mutants.

| Enzyme | K_i (nmol/L) | | | K_i (μ mol/L) |
|--------------------|--------------------------|-------------|-------------|--------------------------------------|
| | Nle ¹ -Ang IV | Ang IV | LVV-H7 | Bestatin |
| IRAP | 150.6±9.2 | 151.7±11.9 | 418.1±27.2 | 231.4±16.0 |
| [A427Y]IRAP | 236.4±18.3 | 208.7±22.1 | 425.6±29.2 | 28.1±3.3* |
| [L483F]IRAP | 1676.5±52.5* | 195.3±39.5 | 881.2±19.1* | >1000** (69% inhibition at 1 mmol/L) |
| [A427Y/ L483F]IRAP | No activity | No activity | No activity | No activity |

Note: Values represent means \pm SE. K_i values were calculated from the relationship $IC_{50} = K_i(1 + [S]/K_m)$. IC_{50} values were determined from at least four individual experiments with duplicate determinations using different concentrations of AT4 peptide inhibitors (10^{-9} – 10^{-4} mol/L) and bestatin (10^{-7} – 10^{-3} mol/L). *, Statistically significant at $p < 0.05$; **, statistically significant at $p < 0.01$ (mutant IRAPs vs the wild type).

Fig. 6. Docking of MCA into the models of wild-type IRAP showed that the interactions were consistent with what has been previously proposed. (A) The proposed catalytic mechanism from Ito et al. (2006). (B) The docking of MCA into the active site cleft of the model of wild-type IRAP in stereo. (C) A diagram of the alternate unproductive docking solution that is observed in the L483F mutant model.



which showed that the double mutant is enzymatically inactive. This suggests that the presence of both mutations likely causes a conformational change that we cannot accurately model.

Discussion

The S1 subsite is occupied by the P1 residue of the N-terminal amino acid of substrates. For LTA4H, this is the same pocket that the phenolic ring of the peptide analog bestatin occupies (Thunnissen et al. 2001). This proposed S1 subsite in LTA4H is a narrow, hydrophobic cavity; in contrast, based on our homology model, the S1 subsite predicted for IRAP is significantly more open in arrangement. This difference is conferred by residues Ala427 and Leu483 in IRAP, corresponding to residues Tyr267 and Phe314, respectively, in LTA4H. LTA4H has no identified endogenous peptide substrates, although it cleaves synthetic arginyl di- and tri-peptides efficiently (Orning et al. 1994). In contrast, IRAP is capable of cleaving a range of small peptides, including peptides with an N-terminal cysteine residue that is part of an intramolecular disulfide loop, namely AVP and oxytocin (Lew et al. 2003; Herbst et al. 1997; Matsumoto et al. 2001).

We demonstrated that the double mutation of the residues Ala427 and Leu483 in IRAP to the corresponding human LTA4H residues inactivated the catalytic activity of the enzyme towards the peptide substrates AVP and Leu-Enk. The lack of activity of the double mutant towards the synthetic substrate Leu-MCA is somewhat surprising because the yeast form of LTA4H, which has the same residues as human LTA4H in the corresponding positions (Y312 and F359), displays characteristics of a leucyl aminopeptidase rather than an arginyl aminopeptidase (Kull et al. 1999). In addition, the mutated IRAP ([A427Y/L483F]IRAP) does not cleave Arg-pNA (results not shown), the preferred synthetic substrate for the aminopeptidase activity of human LTA4H (Orning et al. 1994). Therefore it is likely that, although the double mutation at the substrate-binding pocket altered the conformation of the S1 subsite sufficiently to affect its catalytic activity on certain substrates, there are other determinants within the S1 subsite that affect substrate specificity. The importance of these two residues in defining the catalytic site is underscored by the observation of substrate inhibition for both [A427Y]IRAP and [L483F]IRAP, a phenomenon not observed for wild-type IRAP.

A major effect of the single-point mutation of A427Y in IRAP is a significant increase in the catalytic activity towards the synthetic substrate Leu-MCA, with a rate of cleavage, V , that is 3-fold higher than that of wild-type IRAP, but with no alteration in the substrate affinity K_m . However, the catalysis of the peptide substrate AVP was approximately one third of wild-type activity, whereas the degradation of Leu-Enk was unaltered. We observed marked increases in affinities for both AVP and Leu-Enk of 5- and 26-fold, respectively. Although the changes in the S1 subsite by the A427Y mutation increased the binding affinity for the P1 residue of the peptide substrates (i.e., tyrosine for Leu-Enk and cyclic cysteine for AVP), they also resulted in altered positioning of the peptide substrates to give a conformation that is suboptimal for efficient hydrolysis.

In contrast to [A427Y]IRAP, the substitution of Leu483 with phenylalanine led to a marked decrease in the enzymatic activity assessed using the synthetic substrate. Kinetic studies demonstrated significantly decreased values for both K_m and V , resulting in a marked decrease in the efficiency of hydrolysis (V/K_m) of this mutant enzyme by over 30-fold. The hydrolysis of AVP and Leu-Enk by were markedly different. Whereas [L483F]IRAP was inactive towards Leu-Enk, cleavage of the NH₂-terminal amino acid of AVP (Cyt1) was comparable to wild-type IRAP. The degradation of AVP by wild-type IRAP is a two-stage process because the first cleavage product, Cyt6-AVP(2–9), is also a substrate of the enzyme. [A427Y]IRAP was unable to cleave this Cyt6-AVP(2–9) metabolite. Because the NH₂-terminal amino acid residue for both Cyt6-AVP(2–9) and Leu-Enk is tyrosine, we propose that [L483F]IRAP is unable to orient N-terminal Tyr peptides to the appropriate conformation in the substrate binding pocket for hydrolysis.

The affinities of the peptide inhibitors Ang IV, LVV-H7, and Nle-Ang IV are not altered by the mutation A427Y, which is in accordance with the unaltered K_m observed for the synthetic substrate, because all these compounds have a leucine or a conserved valine at their N terminus. Bestatin, a peptide analog aminopeptidase inhibitor, displays a much higher affinity for LTA4H ($K_i = 0.2 \mu\text{mol/L}$) (Orning et al. 1991) compared with IRAP ($>50 \mu\text{mol/L}$) (Lew et al. 2003). The [A427Y]IRAP mutant displayed a 7-fold increase in affinity for bestatin compared with that of wild-type IRAP, providing strong support for the role of this amino acid residue in providing a suitable S1 subsite for occupation by the N-terminal phenyl group of bestatin. In LTA4H, a ring stack between the tyrosine side chain and the aromatic ring of bestatin has been observed, and we expect that the same arrangement is present in the [A427Y]IRAP mutant, resulting in the marked increase in affinity for bestatin (Thunnissen et al. 2001).

The L483F mutation selectively reduced the affinity of the peptide inhibitor Nle¹-Ang IV for the enzyme, whereas the affinity of Ang IV remained unaltered. The only difference between Nle¹-Ang IV and Ang IV is the N-terminal residue, where the Val¹ (branched, three-carbon side chain) in Ang IV is replaced by Nle¹ (linear four-carbon side chain). Based on these data and the structural analysis performed by Thunnissen and co-workers (Thunnissen et al. 2002), we predict that the peptide inhibitors bind to the catalytic site, with the N-terminal P1 residue occupying the S1 subsite.

The amino acid residues Ala427 and Leu483 of IRAP and the corresponding residues in the other M1 aminopeptidases are consistent with the phylogenetic classification of this family of enzymes (Fig. 2). The corresponding residues in APB are both phenylalanine, indicating that APB and LTA4H form a subfamily within the M1 aminopeptidase family (Tanioka et al. 2003). Both these enzymes possess aminopeptidase activities that preferentially cleave N-terminal arginine and both are inhibited by bestatin at submicromolar concentrations (Orning et al. 1991; Harbeson and Rich 1988; Fukasawa et al. 1996), underscoring the role of these residues in defining the S1 subsite. For the other M1 aminopeptidases (APA, APN), the corresponding residues are conserved with IRAP, i.e., Ala427 and Leu483 (Fig. 3). The

exception is TRH-DE, in which the corresponding residues are valine and phenylalanine, respectively (Fig. 2), and accordingly, this enzyme is positioned between the subfamily of LTA4H/APB and the rest of the M1 aminopeptidases (Tanioka et al. 2003).

In conclusion, we have demonstrated that the residues Ala427 and Leu483 in IRAP play important roles in defining the S1 subsite of the substrate binding pocket, influencing the affinity and orientation of both substrates and peptide inhibitors in the catalytic site. Our data also provide evidence that the peptide inhibitors of IRAP, Ang IV, Nle¹-Ang IV, and LVV-H7, bind to the catalytic site with their NH₂-terminal P1 residue occupying the S1 subsite in a manner similar to that proposed for peptide substrates. These results provide valuable insights into how the different M1 aminopeptidases exhibit substrate specificities and important guidelines for the development of specific inhibitors for the different members of the M1 aminopeptidase family.

Acknowledgements

This research was supported by the Robert J. Kleberg Jr. and Helen C. Kleberg Foundation. S.Y.C. is a Senior Research Fellow with the National Health and Medical Research Council of Australia (NHMRC). D.B.A. is an Australian Postgraduate Award Scholar and a recipient of a St. Vincent's Institute Scholarship. M.W.P. is an Australian Research Council Federation Fellow and NHMRC Honorary Fellow.

References

- Albiston, A.L., McDowall, S.G., Matsacos, D., Sim, P., Clune, E., Mustafa, T., et al. 2001. Evidence that the angiotensin IV (AT4) receptor is the enzyme insulin regulated aminopeptidase. *J. Biol. Chem.* **276**: 48263–48266. doi:10.1074/jbc.C100512200.
- Braszkowski, J.J., Kupryszewski, G., Witczuk, B., and Wisniewski, K. 1988. Angiotensin II-(3–8)-hexapeptide affects motor activity, performance of passive avoidance and a conditioned avoidance response in rats. *Neuroscience*, **27**: 777–783. doi:10.1016/0306-4522(88)90182-0. PMID:3252173.
- Chai, S.Y., Lee, J.H., Matsacos, D., McDowall, S.G., Mendelsohn, F.A.O.M., Robel, P., and Albiston, A.L. 2001. Angiotensin AT4 receptor distribution in mouse brain and its possible role in facilitation of spatial memory. *J. Neurochem.* **78**(Suppl 1): 15.
- Eisenberg, D., Luthy, R., and Bowie, J.U. 1997. VERIFY3D: assessment of protein models with three-dimensional profiles. *Methods Enzymol.* **277**: 396–404. PMID:9379925.
- Fukasawa, K.M., Fukasawa, K., Kanai, M., Fujii, S., and Harada, M. 1996. Molecular cloning and expression of rat liver aminopeptidase B. *J. Biol. Chem.* **271**: 30731–30735. doi:10.1074/jbc.271.48.30731. PMID:8940051.
- Fernando, R.N., Larm, J., Albiston, A.L., and Chai, S.Y. 2005. Distribution and cellular localization of the insulin regulated aminopeptidase (IRAP) in the rat central nervous system. *J. Comp. Neurol.* **487**: 372–390. doi:10.1002/cne.20585. PMID:15906313.
- Harbeson, S.L., and Rich, D.H. 1988. Inhibition of arginine aminopeptidase by bestatin and arphamenine analogues. Evidence for a new mode of binding to aminopeptidases. *Biochemistry*, **27**: 7301–7310. doi:10.1021/bi00419a019. PMID:3207677.
- Herbst, J.J., Ross, S.A., Scott, H.M., Bobin, S.A., Morris, N.J., Lienhard, G.E., and Keller, S.R. 1997. Insulin stimulates cell surface aminopeptidase activity toward vasopressin in adipocytes. *Am. J. Physiol.* **272**: E600–E606. PMID:9142880.
- Hu, X., and Shelver, W.H. 2003. Docking studies of matrix metalloproteinase inhibitors: zinc parameter optimization to improve the binding free energy prediction. *J. Mol. Graph. Model.* **22**: 115–126. doi:10.1016/S1093-3263(03)00153-0. PMID:12932782.
- Humphrey, W., Dalke, A., and Schulten, K. 1996. VMD: visual molecular dynamics. *J. Mol. Graph.* **14**: 27–28, 33–38.
- Ito, K., Nakajima, Y., Onohara, Y., Takeo, M., Nakashima, K., Matsubara, F., Ito, T., and Yoshimoto, T. 2006. Crystal structure of aminopeptidase N (proteobacteria alanyl aminopeptidase) from *Escherichia coli* and conformational change of methionine 260 involved in substrate recognition. *J. Biol. Chem.* **281**: 33664–33676. doi:10.1074/jbc.M605203200. PMID:16885166.
- Krebs, L.T., Kramar, E.A., Hanesworth, J.M., Sardinia, M.F., Ball, A.E., Wright, J.W., and Harding, J.W. 1996. Characterization of the binding properties and physiological action of divalinal-angiotensin IV, a putative AT4 receptor antagonist. *Regul. Pept.* **67**: 123–130. doi:10.1016/S0167-0115(96)00121-8. PMID:8958583.
- Krishnan, R., Hanesworth, J.M., Wright, J.W., and Harding, J.W. 1999. Structure-binding studies of the adrenal AT4 receptor: analysis of position two- and three-modified angiotensin IV analogs. *Peptides*, **20**: 915–920. doi:10.1016/S0196-9781(99)00081-9. PMID:10503768.
- Kull, F., Ohlson, E., and Haeggstrom, J.Z. 1999. Cloning and characterisation of a bifunctional leukotriene A4 hydrolase from *Saccharomyces cerevisiae*. *J. Biol. Chem.* **274**: 34683–34690. doi:10.1074/jbc.274.49.34683. PMID:10574934.
- Lee, J., Albiston, A.L., Allen, A.M., Mendelsohn, F.A.O., Ping, S.E., Barrett, G.L., et al. 2004. Effect of intracerebroventricular injection of AT4 receptor ligands, Nle1-angiotensin IV and LVV-hemorphin 7, on spatial learning in rats. *Neuroscience*, **124**: 341–349. doi:10.1016/j.neuroscience.2003.12.006. PMID:14980384.
- Lew, R.A., Mustafa, T., Ye, S., McDowall, S.G., Chai, S.Y., and Albiston, A.L. 2003. Angiotensin AT4 ligands are potent, competitive inhibitors of insulin regulated aminopeptidase (IRAP). *J. Neurochem.* **86**: 344–350. doi:10.1046/j.1471-4159.2003.01852.x. PMID:12871575.
- Matsumoto, H., Hattori, A., Mizutani, S., and Tsujimoto, M. 2001. Cleavage of peptide hormones by placental leucine aminopeptidase/oxytocinase. In *Cell-surface aminopeptidases: basic and clinical aspects*. Edited by S. Mizutani, A.J. Turner, S. Nomura, and K. Ino. Elsevier Science BV, Amsterdam, Netherlands. pp. 295–299.
- Morris, G.M., Goodsell, D.S., Halliday, R.S., Huey, R., Hart, W.E., Belew, R.K., and Olson, A.J. 1998. Automated docking using a Lamarckian genetic algorithm and an empirical binding free energy function. *J. Comput. Chem.* **19**: 1639–1662. doi:10.1002/(SICI)1096-987X(19981115)19:14<1639::AID-JCC10>3.0.CO;2-B.
- Notredame, C., Higgins, D.G., and Heringa, J. 2000. T-coffee: a novel method for fast and accurate multiple sequence alignment. *J. Mol. Biol.* **302**: 205–217. doi:10.1006/jmbi.2000.4042. PMID:10964570.
- Olson, M.L., Olson, E.A., Qualls, J.H., Stratton, J.J., Harding, J.W., and Wright, J.W. 2004. Norleucine1-angiotensin IV alleviates mecamlamine-induced spatial memory deficits. *Peptides*, **25**: 233–241. doi:10.1016/j.peptides.2003.12.005. PMID:15063004.
- Orning, L., Krivi, G., and Fitzpatrick, F.A. 1991. Leukotriene A4 hydrolase. Inhibition by bestatin and intrinsic aminopeptidase activity establish its functional resemblance to metallohydrolase enzymes. *J. Biol. Chem.* **266**: 1375–1378. PMID:1846352.
- Orning, L., Gierse, J.K., and Fitzpatrick, F.A. 1994. The bifunctional enzyme leukotriene A4 hydrolase is an arginine aminopeptidase of high efficiency and specificity. *J. Biol. Chem.* **269**: 11269–11273. PMID:8157657.

- Pederson, E.S., Harding, J.W., and Wright, J.W. 1998. Attenuation of scopolamine-induced spatial learning impairments by an angiotensin IV analog. *Regul. Pept.* **74**: 97–103. doi:10.1016/S0167-0115(98)00028-7. PMID:9712169.
- Tanioka, T., Hattori, A., Masuda, S., Nomura, Y., Nakayama, H., Mizutani, S., and Tsujimoto, M. 2003. Human leukocyte-derived arginine aminopeptidase. The third member of the oxytocinase subfamily of aminopeptidases. *J. Biol. Chem.* **278**: 32275–32283. doi:10.1074/jbc.M305076200. PMID:12799365.
- Thunnissen, M.M., Nordlund, P., and Haeggstrom, J.Z. 2001. Crystal structure of human leukotriene A(4) hydrolase, a bifunctional enzyme in inflammation. *Nat. Struct. Biol.* **8**: 131–135. doi:10.1038/84117. PMID:11175901.
- Thunnissen, M.M.G.M., Andersson, B., Samuelsson, B., Wong, C.H., and Haeggstrom, J.Z. 2002. Crystal structures of leukotriene A4 hydrolase in complex with captopril and two competitive tight-binding inhibitors. *FASEB J.* **16**: 1648–1650. PMID:12207002.
- Wallis, M.G., Lankford, M.F., and Keller, S.R. 2007. Vasopressin is a physiological substrate for the insulin-regulated aminopeptidase IRAP. *Am. J. Physiol. Endocrinol. Metab.* **293**: E1092–E1102. doi:10.1152/ajpendo.00440.2007. PMID:17684103.
- Wisniewski, K., Borawska, M., and Car, H. 1993. The effect of angiotensin II and its fragments on post-alcohol impairment of learning and memory. *Pol. J. Pharmacol.* **45**: 23–29. PMID:8401756.
- Wright, J.W., Miller-Wing, A.V., Shaffer, M.J., Higginson, C., Wright, D.E., Hanesworth, J.M., and Harding, J.W. 1993. Angiotensin II(3–8) (ANG IV) hippocampal binding: potential role in the facilitation of memory. *Brain Res. Bull.* **32**: 497–502. doi:10.1016/0361-9230(93)90297-O. PMID:8221142.
- Wright, J.W., Stublely, L., Pederson, E.S., Kramar, E.A., Hanesworth, J.M., and Harding, J.W. 1999. Contributions of the brain angiotensin IV-AT4 receptor subtype system to spatial learning. *J. Neurosci.* **19**: 3952–3961. PMID:10234025.